REPORT DOCUMENTATION PAGE

Form Approved OMB NO. 0704-0188

1. REPORT DATE (DD-MM-YYYY)	2. REPORT TYPE	3. DATES COVERED (From - To)
30-09-2012	Final Report	1-Apr-2007 - 30-Jun-2012

4. TITLE AND SUBTITLE
Imaging and Scattering Measurements for Diesel Spray Combustion: Optical Development and Phenomenological Studies

5a. CONTRACT NUMBER
W911NF-07-1-0134

5b. GRANT NUMBER

5c. PROGRAM ELEMENT NUMBER
611102

6. AUTHORS
Jason Porter, Terry Parker, Sean Duran

5d. PROJECT NUMBER

5e. TASK NUMBER

5f. WORK UNIT NUMBER

7. PERFORMING ORGANIZATION NAMES AND ADDRESSES
Colorado School of Mines
Colorado School of Mines
1500 Illinois Street
Golden, CO 80401 -

8. PERFORMING ORGANIZATION REPORT NUMBER

9. SPONSORING/MONITORING AGENCY NAME(S) AND ADDRESS(ES)
U.S. Army Research Office
P.O. Box 12211
Research Triangle Park, NC 27709-2211

10. SPONSOR/MONITOR'S ACRONYM(S)
ARO

11. SPONSOR/MONITOR'S REPORT NUMBER(S)
52247-EG.3

12. DISTRIBUTION AVAILIBILITY STATEMENT
Approved for Public Release; Distribution Unlimited

13. SUPPLEMENTARY NOTES
The views, opinions and/or findings contained in this report are those of the author(s) and should not contrued as an official Department of the Army position, policy or decision, unless so designated by other documentation.

14. ABSTRACT
The first successful demonstration of picosecond ballistic imaging using a greater-than-10 picosecond-pulse-duration laser in diesel sprays is reported. This technique uses an optical Kerr effect shutter constructed from a CS2 liquid cell and a 15 picosecond pulse at 532 nm. The optical shutter can be adjusted to produce effective imaging pulses between 7 and 16 picoseconds. This technique is used to image the near-orifice region (first 3mm) of diesel sprays from a high-pressure single-hole fuel injector. Ballistic imaging of dodecane

15. SUBJECT TERMS
Diesel Injection, Ballistic Imaging, optical diagnsotics of sprays, scattering

16. SECURITY CLASSIFICATION OF:			17. LIMITATION OF ABSTRACT	15. NUMBER OF PAGES	19a. NAME OF RESPONSIBLE PERSON
a. REPORT	b. ABSTRACT	c. THIS PAGE			Terence Parker
UU	UU	UU	UU		19b. TELEPHONE NUMBER: 303-273-3399

Report Title

Imaging and Scattering Measurements for Diesel Spray Combustion: Optical Development and Phenomenological Studies

ABSTRACT

The first successful demonstration of picosecond ballistic imaging using a greater-than-10 picosecond-pulse-duration laser in diesel sprays is reported. This technique uses an optical Kerr effect shutter constructed from a CS2 liquid cell and a 15 picosecond pulse at 532 nm. The optical shutter can be adjusted to produce effective imaging pulses between 7 and 16 picoseconds. This technique is used to image the near-orifice region (first 3mm) of diesel sprays from a high-pressure single-hole fuel injector. Ballistic imaging of dodecane and methyl oleate sprays are reported. The first known ballistic images of diesel injection at pre-ignition engine-like conditions are reported. Dodecane was injected into air heated to 600°C and pressurized to 20 atm. The resulting ballistic images of the near-orifice region at these diesel-engine-like conditions reveal dramatic shedding of the liquid near the nozzle, an effect which has been predicted, but to our knowledge never before imaged. Several parameters are explored including injection pressure, liquid fuel temperature, air temperature and pressure, and fuel type. Resulting trends are summarized with accompanying images. Finally, the beginings of a new ballistic scattering technique is presented with preliminary results.

Enter List of papers submitted or published that acknowledge ARO support from the start of the project to the date of this printing. List the papers, including journal references, in the following categories:

(a) Papers published in peer-reviewed journals (N/A for none)

Received	Paper

TOTAL:

Number of Papers published in peer-reviewed journals:

(b) Papers published in non-peer-reviewed journals (N/A for none)

Received	Paper

TOTAL:

Number of Papers published in non peer-reviewed journals:

(c) Presentations

Number of Presentations: 0.00

Non Peer-Reviewed Conference Proceeding publications (other than abstracts):

Received		Paper
2012/09/30 1	2	S. P. Duran, J. M. Porter, T. E. Parker. Ballistic Imaging of Sprays at Diesel Relevant Conditions, ICLASS 2012, 12th Triennial INternational COnference on Liquid Atomization and Spray SYstems,. 2012/09/02 02:00:00, . : ,

TOTAL: **1**

Number of Non Peer-Reviewed Conference Proceeding publications (other than abstracts):

Peer-Reviewed Conference Proceeding publications (other than abstracts):

Received Paper

TOTAL:

Number of Peer-Reviewed Conference Proceeding publications (other than abstracts):

(d) Manuscripts

Received Paper

TOTAL:

Number of Manuscripts:

Books

Received Paper

TOTAL:

Patents Submitted

Patents Awarded

Awards

Graduate Students

NAME	PERCENT_SUPPORTED	Discipline
Brooke Walters	0.15	
Sean Duran	0.95	
FTE Equivalent:	**1.10**	
Total Number:	**2**	

Names of Post Doctorates

NAME	PERCENT_SUPPORTED
FTE Equivalent:	
Total Number:	

Names of Faculty Supported

NAME	PERCENT_SUPPORTED	National Academy Member
Terry Parker	0.05	
Jason Porter	0.05	
FTE Equivalent:	**0.10**	
Total Number:	**2**	

Names of Under Graduate students supported

NAME	PERCENT_SUPPORTED
FTE Equivalent:	
Total Number:	

Student Metrics

This section only applies to graduating undergraduates supported by this agreement in this reporting period

The number of undergraduates funded by this agreement who graduated during this period:	0.00
The number of undergraduates funded by this agreement who graduated during this period with a degree in science, mathematics, engineering, or technology fields:.....	0.00
The number of undergraduates funded by your agreement who graduated during this period and will continue to pursue a graduate or Ph.D. degree in science, mathematics, engineering, or technology fields:.....	0.00
Number of graduating undergraduates who achieved a 3.5 GPA to 4.0 (4.0 max scale):	0.00
Number of graduating undergraduates funded by a DoD funded Center of Excellence grant for Education, Research and Engineering:	0.00
The number of undergraduates funded by your agreement who graduated during this period and intend to work for the Department of Defense	0.00
The number of undergraduates funded by your agreement who graduated during this period and will receive scholarships or fellowships for further studies in science, mathematics, engineering or technology fields:	0.00

Names of Personnel receiving masters degrees

NAME
Brooke Walters
Total Number: 1

Names of personnel receiving PHDs

NAME
Total Number:

Names of other research staff

NAME	PERCENT_SUPPORTED
Chris Dryer	0.02
FTE Equivalent:	**0.02**
Total Number:	**1**

Sub Contractors (DD882)

Inventions (DD882)

Scientific Progress

The first successful demonstration of picosecond ballistic imaging using a greater-than-10 picosecond-pulse-duration laser in diesel sprays is reported. This technique uses an optical Kerr effect shutter constructed from a CS2 liquid cell and a 15 picosecond pulse at 532 nm. The optical shutter can be adjusted to produce effective imaging pulses between 7 and 16 picoseconds. This technique is used to image the near-orifice region (first 3mm) of diesel sprays from a high-pressure single-hole fuel injector. Ballistic imaging of dodecane and methyl oleate sprays are reported. The first known ballistic images of diesel injection at pre-ignition engine-like conditions are reported. Dodecane was injected into air heated to 600°C and pressurized to 20 atm. The resulting ballistic images of the near-orifice region at these diesel-engine-like conditions reveal dramatic shedding of the liquid near the nozzle, an effect which has been predicted, but to our knowledge never before imaged. Several parameters are explored including injection pressure, liquid fuel temperature, air temperature and pressure, and fuel type. Resulting trends are summarized with accompanying images. Finally, the beginings of a new ballistic scattering technique is presented with preliminary results.

Technology Transfer

Final Report - Grant # W911NF-07-1-0134
(Reporting Period: September 2009 – August 2012)

Imaging and Scattering Measurements for Diesel Spray Combustion Optical Development and Phenomenological Studies

Terry Parker, Jason Porter
Mechanical Engineering Department
Colorado School of Mines, Golden, CO, 80401

Table of Contents

Abstract

The first successful demonstration of picosecond ballistic imaging using a greater-than-10 picosecond-pulse-duration laser in diesel sprays is reported. This technique uses an optical Kerr effect shutter constructed from a CS_2 liquid cell and a 15 picosecond pulse at 532 nm. The optical shutter can be adjusted to produce effective imaging pulses between 7 and 16 picoseconds. This technique is used to image the near-orifice region (first 3mm) of diesel sprays from a high-pressure single-hole fuel injector. Ballistic imaging of dodecane and methyl oleate sprays are reported. The first known ballistic images of diesel injection at pre-ignition engine-like conditions are reported. Dodecane was injected into air heated to 600°C and pressurized to 20 atm. The resulting ballistic images of the near-orifice region at these diesel-engine-like conditions reveal dramatic shedding of the liquid near the nozzle, an effect which has been predicted, but to our knowledge never before imaged. Several parameters are explored including injection pressure, liquid fuel temperature, air temperature and pressure, and fuel type. Resulting trends are summarized with accompanying images. Finally, the beginings of a new ballistic scattering technique is presented with preliminary results.

1. Introduction

This effort is focused on a combination of developing the optical tools to probe the high-density region of a diesel spray and the use of these tools to improve our understanding of the near-orifice spray behavior. Near-orifice images provide a valuable benchmark data set for development of advanced atomization and spray models. This work is based on a unique capability developed at CSM relevant to improvements in diesel engine technology. This experimental capability includes the ability to produce very controlled, diesel-like pre-injection conditions along with non-intrusive diagnostics specifically developed to monitor the near field of diesel sprays. Continued work is focused on ballistic imaging improvements, including a shift from line-of-sight measurements to spatially resolved measurements, and establishing an archival quality data set of the effects of fuel type, injector type, temperature and pressure on the near-orifice of diesel sprays. The purpose of the facility and diagnostics being to investigate the controlling breakup modes of diesel sprays for operating ranges relevant to diesel engines.

1.1 Motivation

Research efforts have focused on the implementation of the ballistic imaging technique to probe structures in the near-orifice region of high-pressure diesel sprays. The motivation to choose ballistic imaging stems from the desire to reveal intricate spray structures which otherwise are not discernible via other methods. Through the use of an ultra-fast shutter, the ballistic imaging technique captures photons that have passed through an optically dense spray with minimal, if any, scattering events. The lack of scattering is vital to retaining the true structure of the spray, as scattered photons blur the image and act to conceal the complex structures on the periphery of the spray. The detailed structures captured in these ballistic images will help improve spray breakup models by providing experimental evidence for comparison with simulations. Improved understanding of the break-up region of fuel sprays enables better control of droplet size

distribution, evaporation, and downstream mixing in diesel sprays, with potentially profound implications for improved diesel cycle efficiency and reduced emissions.

Measurements in diesel sprays are ideally non-intrusive and typically rely on laser interactions with the droplet field; therefore, measurements close to the injector tip must be able to monitor droplet sizes in spite of high number densities and high levels of attenuation [1]. Techniques such as Phase/Doppler measurements [2], [3] or imaging measurements that rely on separate images of droplets [4] are ineffective near the injector orifice due to multiple scattering in the overall system. Signal attenuation for ensemble light scattering techniques utilizing visible wavelengths makes these techniques of marginal use in the dense spray [5], [6]. Diffraction based instruments [7] with obscuration levels greater than 50% require empirical or theoretical corrections [8], while polarization ratio measurements [6] can be insensitive to optical depth but have a limited dynamic range. Finally, x-ray imaging of fuel sprays has been applied to the near-orifice of non-evaporating fuel sprays to measure fuel mass fraction [9], fuel velocity fields [10], the influence of gas density on penetration length, and the internal structure of the nozzle [11]. However, challenges with this technique include the need for tracer seeding for adequate absorption of x-ray radiation, a limited potential for wider engine studies given the need for an x-ray synchrotron, and to date, no x-ray imaging has been reported on evaporating or combusting fuel sprays. In addition, recent modeling of phase-contrast x-ray imaging suggests significant challenges in imaging dense sprays [12].

Ballistic imaging offers an opportunity to investigate the optically dense region of the spray by producing shadowgraph- or schlieren-style images of structures that are embedded inside a turbid field. Identifying embedded structures is especially relevant given conflicting predictions of both a negligible liquid core [8] and a core of up to 100 jet diameters in length [13]. Work at CSM has documented the utility of the ballistic imaging technique for dense sprays [14], [15] and work at CSM with diesel sprays injected into an ambient atmosphere indicate very significant mixing structures on the spray periphery [16], [17].

2. Experimental Methods

Ballistic imaging is applied to the near-orifice region and provides line-of-sight images of the spray “interior”[13]. The ballistic technique relies on an ultrafast laser system and high speed shuttering to separate ballistic photons that carry image content from the multiply scattered photons that are not useful for reconstructing the characteristics of the spray field. Efforts at CSM have focused on the development of picosecond ballistic imaging, where a picosecond laser is used instead of the more expensive femtosecond laser [15], as well as applying ballistic imaging to diesel sprays in diesel-engine-like conditions (high temperature and pressure).

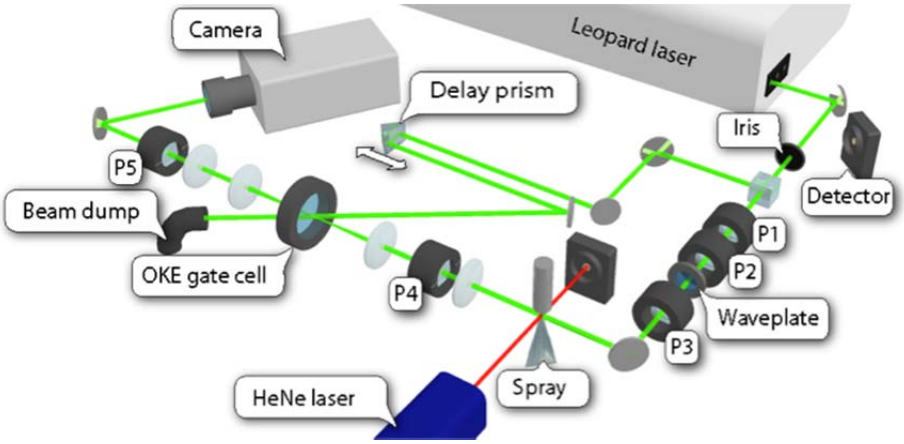

Figure 1: Experimental schematic of ballistic imaging optical train. The HeNe laser and separate detectors are to measure the arrival of the imaging pulse and the spray injection timing. P1-P5 are polarizers. Beams are shown cw for clarity.

2.1 Ballistic Imaging Optical Train

An experimental schematic is shown in Figure 1 with the 532nm output from a Coherent Leopard D-10 laser operating at 10 Hz repetition rate with 12±1 mJ per pulse used as the basis for the measurement. As shown in the diagram, the laser was split into an OKE (optical Kerr effect) gate beam and an imaging beam with a 90/10 cube beam splitter; the higher energy pulse was used to produce the OKE gate beam. The OKE gate beam traveled across the table to a prism mounted on a translation stage and was then directed through a CS_2 cell. This part of the system is known as the delay line and is used to produce an overlap, in space and time, of the gate beam and the imaging beam (see Figure 3). The OKE gate was formed by a pair of crossed polarizers, P4 and P5, and the OKE gate cell. P4 was oriented to pass the non-scattered image beam, while the output linear polarizer (P5) of the OKE gate was set to be crossed with P4. The key to the time gating is the rotation of the polarization state of the image beam, which is the result of the interaction of the gate beam in the carbon disulfide.

2.2 Image Capture

In order to take images inside the pressure vessel, a timing scheme was designed to sync the laser pulse with the camera system and the injector firing. The laser outputs a weak electrical pulse a few microseconds before each laser pulse. This pulse is not sufficient to trigger most electronics, initial efforts used an HP® pulse generator to convert the weak pulse to a TTL signal which has sufficient power to trigger multiple devices. However, the variation in timing between the generation of this pulse and the the production of a laser pulse was sufficiently large (~1 millisecond) that we moved to a system that used a photodiode that sensed the laser pulse based on reflection from an optical interface as the trigger pulse for the event. Again, a pulse generator was used to provide signal pulses based upon the "trigger" event which is the pulse from the laser. This 10 Hz pulse train is fed to a custom programmed PIC controller box which receives the laser timing pulse waits for the operator to fire the injector. If there is no request for injection, as one would expect, there is no further action from the controller. Upon receiving a request for an injection event, the RS232 word (this word includes instructions for the injection event that determine the injection duration and/or parameters for multiple injections spaced over a period of 10 or so milliseconds) is transmitted from the controlling computer to the PIC where it is held

until the next laser pulse is detected. Using this laser pulse as t=0, the PIC releases the word after 20 ms to the injector controller; the injector controller subsequently fires the injector. By adjusting the delay between the laser pulse sensed by the photodiode and the output pulse from the signal generator, the user can control the arrival time of the laser pulse in the spray with respect to the beginning of the injection event. In addition to transmitting the binary word to the injector controller, the PIC also sends a TTL pulse to the camera which effectively produces an "image capture" signal that envelopes the time period when the laser pulse is present. This pulse is delayed via a second pulse generator. BY utilizing both pulse generators the user can adjust the timing of the image in the spray, relative to the beginning of the spray.

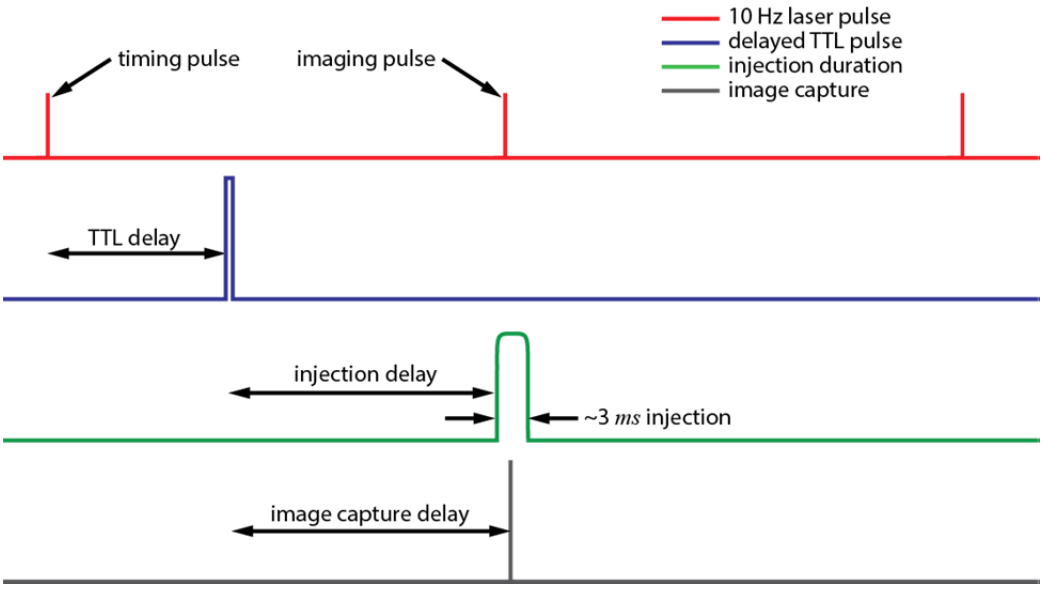

Figure 2: A schematic of the electronic timing used during imaging.

The camera is a Photometrics Cascade:650 imaging array (653x492 pixels, each of which is a 7.4 μm square). This camera is designed for low-light applications, and was used in conjunction with an ND 2.0 filter and a 532 nm band pass filter to optimize signal levels and to filter stray light. Spray duration is tracked using a HeNe laser beam aligned to cross directly below the tip of the injector. The HeNe beam is directed to a detector and monitored on an oscilloscope. Spray duration as determined by attenuation of the HeNe beam is typically 3.0 to 3.5 ms. The imaging beam is monitored via a photo detector on the same oscilloscope. The arrival time of the imaging beam relative to the initiation of the spray is determined from the oscilloscope traces.

2.3 Continuum® Leopard Picosecond Laser

The illumination for the images is provided by a Continuum® Leopard D-10 laser, which operates at 10Hz. This is a powerful laser capable of 30mJ, 15 picosecond pulses at 1064nm. Compared to the femtosecond lasers used by other groups to achieve ballistic images, this setup only requires one laser to operate. The Leopard is a cheaper and much more robust system capable of emitting pulses at 266, 355, 532 and 1064nm. This multi-wavelength capacity lends more diagnostic capacity to the user. However, given the pulse duration and the usage of a saturable absorber, this laser is a very low production unit which is nominally manufactured at a

rate of one laser per year. Because of this there is not a large user group for the laser and the service requirements for this laser can be difficult to meet.

The low production quantity, and the novel way the laser is being employed have revealed issues that more traditional users may not encounter. For example, issues have come up in several areas of operations including evaporation of the dichloroethane from the dye circulator. The original design was poorly sealed and leaked the carcinogenic vapors into the lab. A custom, in-house design was built and incorporated Swagelock® fittings and appropriate O-ring seals to minimize the escape of vapors. In addition to stopping the leakage, the design had the effect of prolonging the life of the saturable absorber. This is beneficial since tuning the dye is a time-consuming undertaking. A second issue is the focusing of the beam at a range of 10 meters. This is difficult to adjust, as the laser has no provisions for adjustment of its telescoping optics. In order to collimate the beam, the user must remove the rear folding optic and replace it with one with a different focal length. This is an expensive and time-consuming process which requires amplifier alignment with each adjustment.

Another issue is the laser's poor pointing stability. Measurements have revealed that the laser has a horizontal drift of 400 microradians and a vertical drift of 250 microradians. This drift is a source of noise in our measurements and conversations with the manufacturer have not yet yielded a solution to the problem. We are continuing to work with the manufacturer to bring this laser into "specification" which was a factor of 50 or so smaller than the pointing stability behavior that we have observed.

A second-generation model of this laser which addresses these and potentially other issues would make for a simpler, more turn-key operation. This contrasts with the current situation, which requires an extensive overhead of operator knowledge, which is not easily conferred to a new user.

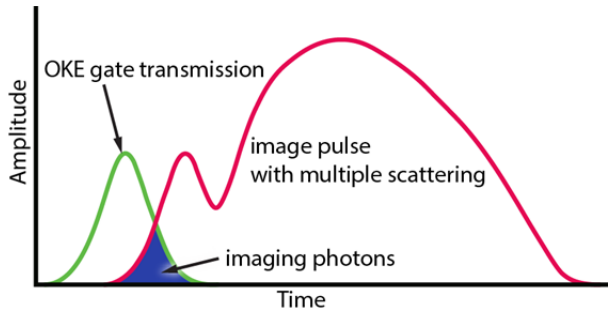

Figure 3: Schematic diagram of the time overlap of the optical kerr effect shutter and the image pulse that passes through the gate. Changing this overlap in time effectively changes the "on" time for the shutter.

2.4 Optical Kerr Effect Shutter

Picosecond ballistic imaging, also referred to as "pulse-sliced" ballistic imaging, relies on precise timing of the optical Kerr effect shutter. The OKE gate beam can be delayed relative to the arrival of the imaging pulse as shown schematically in Figure 3. The imaging pulse arrives after the OKE gate is turned "on" by the OKE gate pulse. By varying the timing of the gate beam, the quality of the images can be adjusted to let more or less scattered photons onto the image plane during capture. Figure 3 depicts a stylized cartoon of the basic effects of gate and image beam overlap (shown in blue) in picosecond ballistic imaging. If the gate beam arrives too early, the

overlap area is reduced and too few photons reach the camera resulting in a poor image. Alternatively, if the gate beam arrives too late, the overlap area is large but includes a large percentage of scattered photons, blurring the image. The best results achieved to date are with the Kerr Cell transmission switching "off" just as the image pulse arrives at the Kerr cell. Subtle changes in the timing of the imaging and gating beams utilized to capture these images can result in ballistic vs. non-ballistic results [Figure 4].

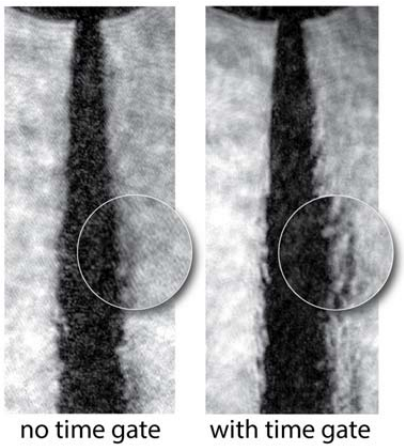

Figure 4: Example of ballistic vs. non-ballistic spray images.

For an example of the effects of gate position, consider Figure 5, which shows three spray images captured at a similar time during the spray event. In this figure, the degradation in image quality is visible as more scattered photons are allowed to pass onto the image plane by adjusting the overlap of the gate and image beams. The best images are captured when the gating beam reaches the optical shutter first allowing the shutter to close at the appropriate time (a,b). As the gate beam's arrival is delayed, the shutter is open at a non-optimal time and the image suffers a blurring effect, which removes the clarity of the peripheral structures (c).

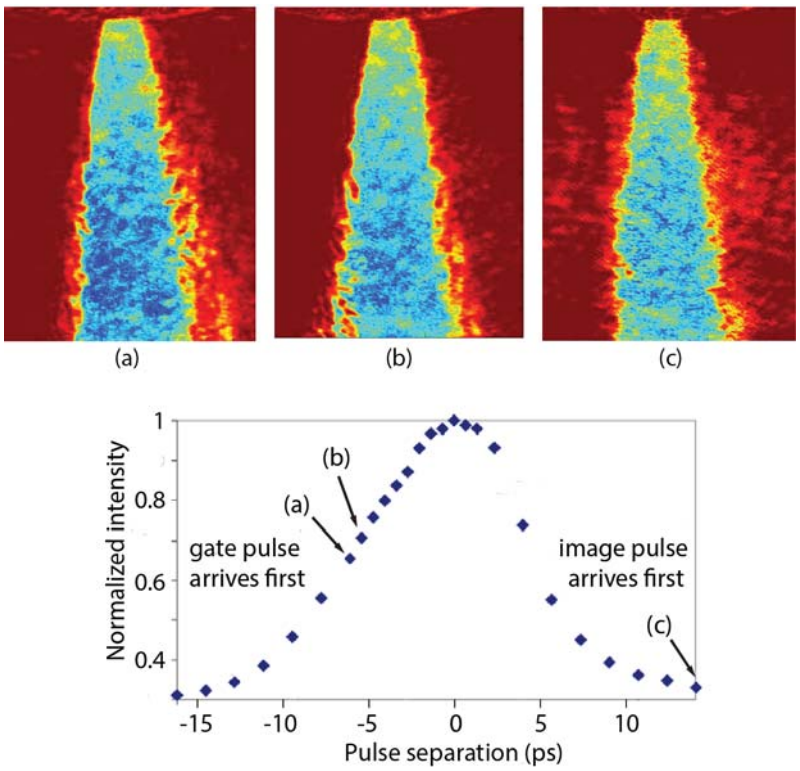

Figure 5. (Top) Images demonstrating the effect of overlap timing on image quality. (a) Image arrives 6.7 ps after gate beam. (b) Image arrives 5.0 ps after gate beam. (c) Image arrives 14.7 ps before gate beam. Color scale added for effect. (Bottom) A graph of measured transmission versus gate pulse and image pulse temporal separation.

The use of "pulse-slicing" to improve the image by aggressively eliminating scattered photons is limited by the Gaussian nature of the pulse and also the number photons available in the pulse slice. A property of the Gaussian function is that the product of a two identical Gaussians produces a Gaussian with a width that decreased by a factor which is one over the square root of two. Thus, if the laser pulse is a perfect Gaussian, pulse slicing can at best produce a square root of two decrease in effective pulse duration. In fact we have seen decreases in pulse width that are greater than this which we attribute to the non-ideal nature of the pulse. However, this does illustrate that our ability to move from a 12-14 psec parent laser pulse to an effective image pulse that is in the 2 picosecond range will require a gating scheme that not only turns the OKE gate "on" with a pulse, but also turns it off with a second pulse. In addition, as we have aggressively moved to lower levels of overlap between the image and gate pulse, image quality decays simply because of the smaller number of photons available (this is due both to the photon statistics associated with a small number of photons and equally important, that as the signal level approaches the background level of the measurement, separation of signal from background becomes dominated by noise).

Putting aside the timing variables associated with the OKE gate, the key to taking quality images is a well-designed optical system. To achieve this, an optical train was designed using Zemax© software resulting in a spatial resolution of approximately 20 microns. The use of Zemax allowed for considerable flexibility in choosing components, which were well suited to our application. The finalized design utilized achromatic lenses, which minimize chromatic and spherical aberrations in the imaging train and allow for the best achievable resolution. As in most systems, the quality of the image was influenced the most by the lowest quality optic in the

assembly, in this case the cell used to hold the CS_2 Kerr medium. Initially, the CS_2 was contained in a rectangular colorimeter cell with a custom built Teflon cap to alleviate the evaporation of the hazardous chemical. Images with and without the cell were drastically different, with the old cell producing serious resolution degradation. This problem was resolved via the manufacture of a custom containment cell, which both improved the optical quality of the system and eliminated the evaporation of CS_2 into the lab environment. A comparison of the Standard Air Force target images for the two cases is presented in Figure 6. The original colorimeter's maximum resolution was (group 3-element 4) 11.3 line pairs per millimeter, whereas the optical windows resolved 40.3 lp/mm (group5-element 3).

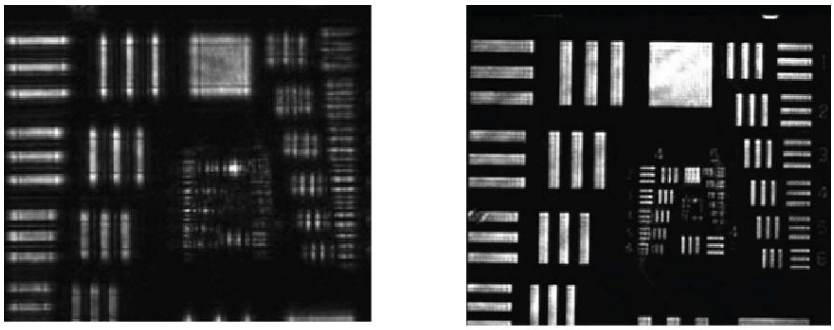

Figure 6: A comparison of the image quality between the older colorimeter cell (a) and the new containment cell (b).

2.5 Autocorrelation-Based Pulse Length Measurements

A significant issue with using the Continuum Leopard laser for ballistic imaging has been quantifying the "on-time" duration produced by overlapping the imaging beam with the gate (or switching) beam. Since the imaging beam is not transmitted through the OKE gate unless the gate beam activates the carbon disulfide, the level of overlap should control the on-time and transmission level for the gate. The Continuum Leopard laser has a second harmonic pulse length of 14 ps. Thus the gate beam provides a 14 ps window for the imaging pulse to be transmitted through the OKE. In contrast, femtosecond lasers produce an OKE "on" time that is controlled by the relaxation time for the carbon disulfide (~2 ps).

To fully quantify the pulse length from the laser a long-scan autocorrelator was utilized, with this autocorrleator specifically designed for a low pulse frequency laser (i.e. 10 Hz). The autocorrelator was selected since the pulses are picoseconds in duration, which is too short for any electrical measurement systems. Autocorrelation measurements are taken by splitting the desired pulse into two separate beams which are recombined within a doubling crystal. By moving one of the pulses relative to the other via a translation stage, the beams are allowed to interfere with one another within the crystal. The output from the doubling crystal is captured on a high-speed photodiode and the diodes response is sent to a gated integrator. Since any photosensor used to detect the laser pulse will produce a signalt that is the impulse response of the system, an integrated measurement is used which captures the entirety of the impulse response and this integrated signal is directly proportional to the energy level incident on the photodetector.

Careful scanning of the delay time for one pulse in the autocorrelator with respect to another, with signals acquired for each delay time, produces a record of signal versus delay time [Figure

5]. This signal can be processed to produce the length of the original laser pulse. We have tested this system with the original pulse from the laser and then used the same system to determine the pulse duration for a signal that passes through the OKE cell. By managing the overlap between gate and image pulse, we have produced a transmission "on" time of approximately 8.5 ps.This result is shown in Figure 7, which illustrates OKE "on" time as a function of gate beam energy. Note the slight dependence on the gate beam energy and that the transmission level for the OKE gate is quite high.

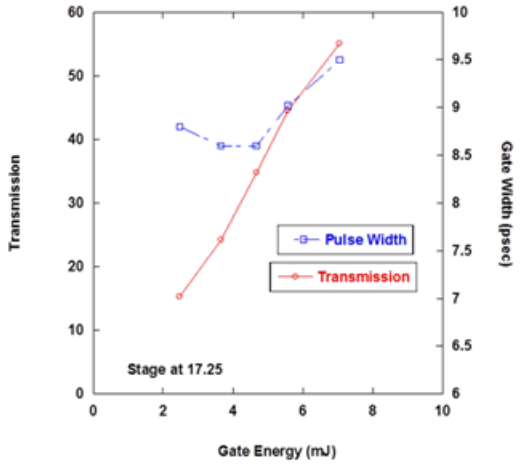

Figure 7: Performance of the OKE gate with the gate beam arriving at the Kerr cell 8.2 ps before the image beam.

An issue which has arisen during this examination is the response time of the integrator to the triggering signal. The delay between trigger signal and start of the integration is tens of nanoseconds which is greater than the propagation delay in normal length electrical cable. In order to synchronize the fast response of the photodiode with the gated integrator requires the creation of a delay in the signal. The majority of the measurements taken during this experiment used cabling to delay the signal from the photodiode, which introduced larger than desired capacitance into the system. This increased capacitance resulted in pulse elongation and issues with non-linearity. A second method of introducing a delay was to increase the optical pathlength, after the trigger photodiode signal creation point, by sending the laser pulse across the lab to create the same delay as the cable method. This method proved to be problematic due to the pointing stability issues mentioned in the discussion about the laser. The pointing issue caused very poor signals because the beams were wandering within the autocorrelator creating fluctuations in the measured signal. We continue work with the vendor on the pointing stability of the laser system and expect the ultimate solution to be a combination of better pointing stability and an amplifier on the trigger signal that introduces some delay into the system.

Using the cable method and a more efficient doubling crystal, measurements of the native pulse yielded FWHM duration of 14ps. At an optimal image and signal beam overlap, preliminary autocorrelation traces suggested the sliced pulse had FWHM duration of between 6-8ps.

2.6 Diesel Injection System

In order to provide the liquid injections needed for imaging, a Sturman® Industries common-rail type diesel injector is utilized. This injection system is capable of multiple pulse injections with

pressures in excess of 200 MPa. This system uses a hole-type nozzle, which is custom drilled to include a single, on-center, injection hole. The injector was designed for a dynamic environment in which fuel and high-pressure oil are constantly being cycled through the injector body. The high-pressure oil, which drives the injection events, is normally driven out the top of the injector where it would be contained by an engine's valve covers before being returned to the sump. However, in an optics laboratory, high-pressure oil being ejected into the atmosphere is problematic. To mediate the contamination risk, the injector body itself has been modified with an O-ring sealed manifold to route the used oil into a containment vessel.

Of additional concern is fuel coking due to the fuel standing in the injector head for extended periods at high temperature. To prevent fuel degradation and subsequent clogging of the injector, the injector body has been encapsulated in an insulated protective housing. Modeling of the thermal conditions has revealed that the injector tip assembly maintains a maximum temperature of about 150ºC. Cooling of the fuel is enhanced by recirculation of the fuel through the injector housing and into a cooling bath utilizing a coil-type heat exchanger. Examination of the disassembled injector shows no signs of fuel coking (normally observed at 150-180ºC), even after operation at chamber temperatures of 600ºC.

2.7 Diesel Engine Simulator

Experiments utilize a custom-manufactured combustion vessel capable of maintaining pre-injection conditions at 50 atm and 1000 K. As shown in Figure 8, the diesel engine simulator was split into an inner heated core surrounded by an exterior pressure vessel. The exterior pressure vessel has four orthogonal, purged optical ports for line-of-sight optical measurements and detection at 90º. The inner heated core is the central air-bearing region and is 44.5 mm in diameter. The distance from the injector tip to the opposing wall is adjustable. Further details of the experimental system and gas extraction can be found in the literature [12] and are summarized in Table 1.

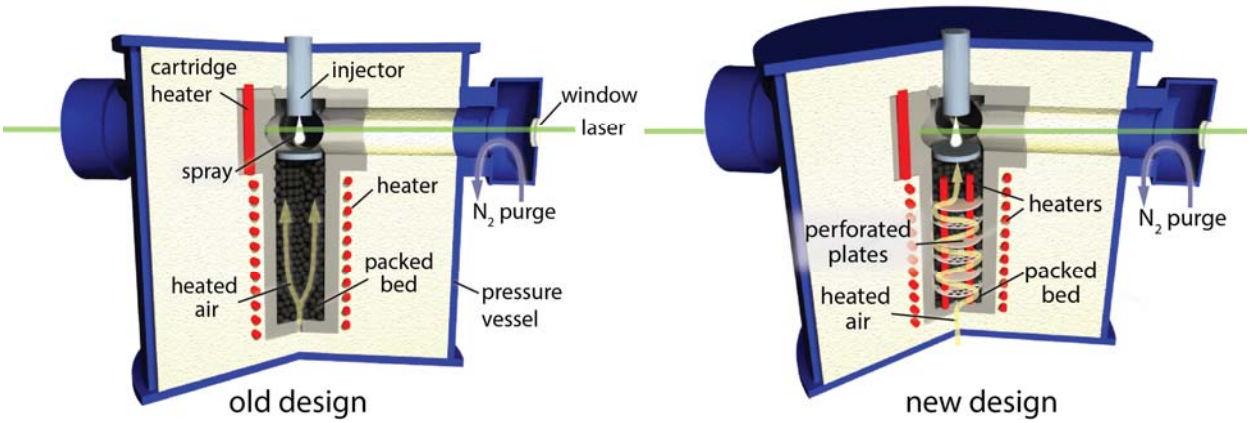

Figure 8: The Diesel Engine Simulator. New design increases air residence time in packed bed for better air temperature control.

Due to the range of engine designs and operating conditions there is no "standard" diesel combustion event. Experiments conducted in the simulator described in this paper are designed to emulate a number of the important characteristics of diesel combustion. As shown in Table 1, the simulator effectively replicates most of the important characteristics of diesel combustion.

The most striking difference between the simulator and engines, in terms of operating parameters, is pressure. The simulator was operated at 20 atm versus the 30 atm and greater typical of diesel engines; additionally, the simulator is isobaric.

Table 1. Comparison of typical diesel engine characteristics with the Diesel Engine Simulator.

Characteristic	Engine	Simulator (for most recent work)
Injection Pressure	30-150 MPa[18], 20-80 MPa[18], 100-150 MPa[19], 20-170 MPa[20]	55-150 MPa
Nozzle orifice diameter	0.15-0.35 mm [18], 0.184 mm[19], 0.194 mm	0.160 mm
Nozzle orifice L/D	2-8[20], 4	4
Number of nozzle orifices	3-8 holes	1 hole
Types of nozzles used	Pintle and Hole-type nozzles	Hole-type nozzle
Mass injection	2-24 mm^3 per hole[21]	4 mm^3 min.; 37 mm^3 max.
Chamber Temperature	1000-1200 K, 700-1300 K [22]	873 K
Chamber Pressure	40-120 atm [18], 50-100[20]	20 atm (plans for 35 atm)
Hard wall interaction length	50-60 mm[22]	100 mm
Liquid Length	18 mm[1]	30 mm
Change in Chamber Pressure	6 MPa[22]	25 kPa
Compression Ratio	16-22[20]	None
Overall Stoichiometry	Fuel Lean[20]	Fuel Lean

Extended usage of the high-pressure facility has brought some design issues to light and has prompted a redesign of the heater controls and heating element placement. The redesign supplements the lower clamshell heater with four interior cartridge heaters [Figure 8]. This has the advantage of increasing the amount of heat, which can be added to the incoming air from 350W to 1400W. Perforated plates were also added to the packed bed to improve distribution of the incoming air enhancing heat transfer between the cartridge heaters and the air. Additionally, each of the cartridge heaters was manufactured with a thermocouple built into its tip. The placement of the thermocouple in the tip of the heater allows for more precise temperature control since the temperature is measured in the flow rather than the previous location in the inner wall of the vessel. The more precise temperature control and the new design of the packed bed heater will create more rapid and uniform heating of the gas flow. The benefit of uniform heating will be images that are less likely to be degraded by thermal gradients. Additionally, the nitrogen purge used to keep the optical access windows clean will be preheated to further reduce thermal gradient blurring of images.

2.8 Image Processing

In order to create an image of optical depth, a series of image processing steps are undertaken for each image [Figure 9]. Prior to capturing spray images, a series of images are taken with the lens cap on the camera (background images). Additionally, images are captured of the laser with no spray, which constitutes the baseline images. These series of images are then averaged and are labeled background (B) and baseline (I_0) respectively. Finally, the image of the spray is captured (labeled I in Figure 9). Using $-\ln(\frac{I-B}{I_0-B})$, a background subtracted optical depth image is created. The optical depth image is then contrasted to enhance its features.

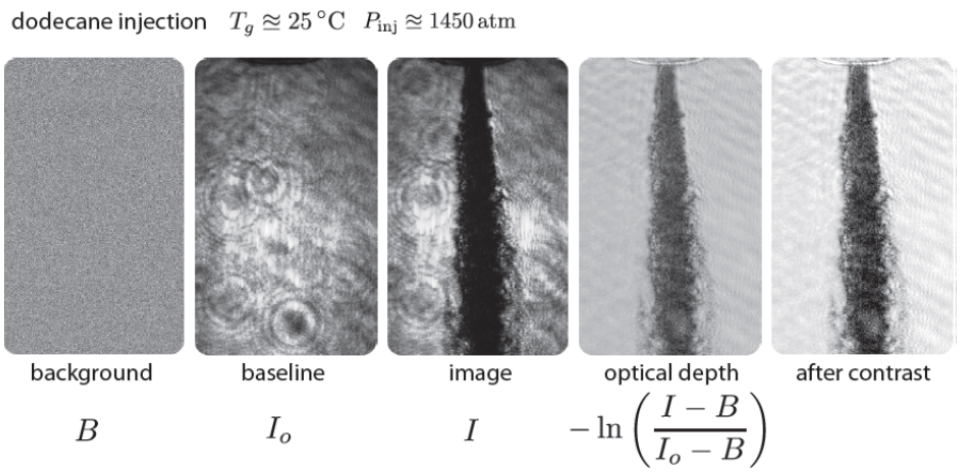

Figure 9: A visual guide to the image processing steps used in capturing ballistic images of sprays.

3. Diesel Spray Imaging Results & Discussion

Two types of fuels have been investigated in this program, dodecane and methyl oleate. Dodecane is a common diesel fuel surrogate and methyl oleate is a common bio-diesel surrogate. Several different test regimes were examined and will be presented individually and then compared in terms of observed trends. These include:

- Dodecane injected into ambient air at varying injection pressure (Table 2. Rows 1-2)
- Dodecane injected into room-temperature air at elevated air pressures (Table 2. Row 3)
- Dodecane injected into air at elevated temperature and pressure (Table 2. Rows 4-6)
- Methyl oleate injected into ambient air (Table 2. Row 7)

Table 2. Table of some of the fuel conditions tested, corresponding fuel properties [23][24][25], and non-dimensional groups.

		temp (liq) (°C)	temp (charge) (°C)	pressure (charge) (atm)	pressure (injection) (atm)	velocity (m/s)	liquid density (kg/m^3)	surface tension (N/m)	liquid viscosity (Pa-s)	Re (-)	We (-)	Oh (-)
dodecane	1.	25	25	1	970	514	744.4	2.49E-02	1.32E-03	4.65E+04	1.26E+06	2.41E-02
	2.	25	25	1	1500	639	744.4	2.49E-02	1.32E-03	5.79E+04	1.95E+06	2.41E-02
	3.	25	25	20	1450	623	745.8	2.49E-02	1.35E-03	5.52E+04	1.86E+06	2.47E-02
	4.	150	600	3	1450	672	650.0	1.39E-02	3.21E-04	2.18E+05	3.38E+06	8.45E-03
	5.	150	600	12	1450	669	651.5	1.39E-02	3.26E-04	2.14E+05	3.36E+06	8.57E-03
	6.	150	600	20	1450	666	652.7	1.39E-02	3.30E-04	2.11E+05	3.35E+06	8.67E-03
methyl oleate	7.	25	25	1	1450	581	868.8	2.90E-02	5.32E-03	1.52E+04	1.62E+06	8.38E-02

For reference in comparing imaging results from different fuels and conditions, Table 2 has been compiled, which contains the majority of the experimental conditions with accompanying fuel properties and non-dimensional groups. Reynolds, Weber, and Ohnesorge numbers were evaluated using the following equations from fuel properties and injection parameters [26].

$$\mathrm{Re} = \frac{\rho_l L V}{\mu_l}, \quad \mathrm{We} = \frac{\rho_l L V^2}{\sigma}, \quad \mathrm{Oh} = \frac{\mathrm{We}^{1/4}}{\mathrm{Re}} = \frac{\mu_l}{(\rho_l \sigma L)^{1/4}}$$

where ρ_l, μ_l, σ, and V, are the density, viscosity, surface tension, and velocity of the liquid fuel, and the characteristic length, L, was taken as the injector orifice diameter: 0.16 mm. The velocity was calculated from Bernoulli's equation. The Reynolds number relates the ratio of inertial to viscous forces and the Weber number relates the ratio of momentum to surface tension forces and has been correlated with jet breakup regimes. The Ohnesorge number is given by the ratio of the fourth root of the Weber number and the Reynolds number and is an indicator of jet stability.

Some trends are immediately obvious from the data in Table 2. First, fuel properties are largely insensitive to the charge pressure (vessel pressure). On the contrary, fluid temperature has a more dramatic effect on density, surface tension, and viscosity. The Weber number nearly doubles as the fuel liquid temperature rises from ambient to 150°C, while the Ohnesorge number is reduced by a factor of three for the same temperature change. The most significant change in fuel properties is the reduced viscosity at high temperature. This reduction in viscosity could in part explain the observed shedding structures seen in high temperature and pressure dodecane sprays discussed below.

3.1 Transient Fluctuations in Room Temperature Dodecane Sprays

The bulk of the initial imaging undertaken in this study was of dodecane at standard temperature and pressure. This phase of testing was focused on validating the system's performance and provided proof of concept testing for pulse-sliced ballistic imaging. These initial images revealed trends in the spray, which were present across the entire test matrix of fuels, temperatures and pressures. The most important trend observed in this phase of testing was the oscillation of the width of the spray in time [Figure 10]. Similar oscillations have been seen in all cases studied.

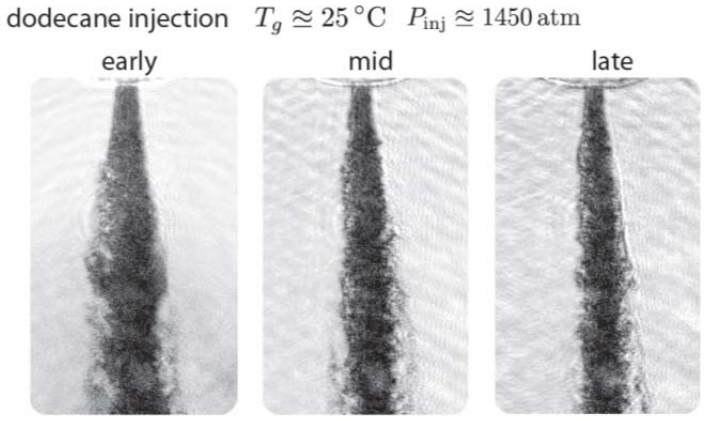

Figure 10: Images at different times in the dodecane spray.

3.2 Injection Pressure and Double Pulsed Injection

In a separate experiment, the injection pressure of dodecane was varied from 970 to 1500 atm to examine the effects on the spray structure. This study revealed that at all three injection pressures, significant shedding was present on the spray's periphery [Figure 11]. Also, there was a slight narrowing of the spray cone angle with increasing injection pressure [Figure 12].

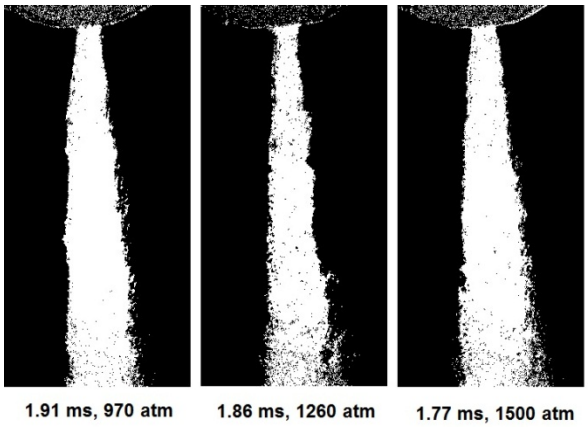

Figure 11: Binary images of dodecane at various injection pressures reveals significant shedding in all cases.

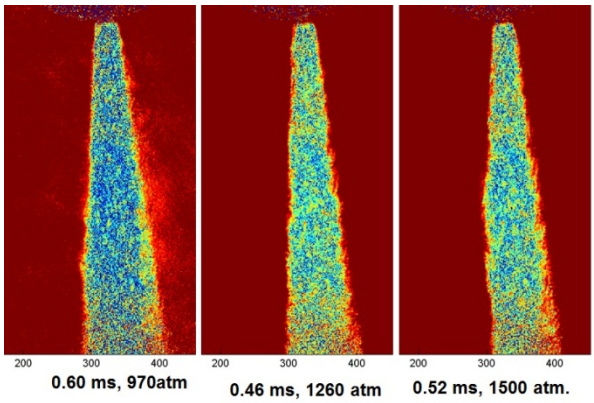

Figure 12: Color mapped images captured early in the spray reveal a reduction in cone angle with increasing pressure.

In yet another experiment, the injector was double-pulsed into atmospheric conditions. This test was made to examine the effects of multiple injections in rapid succession, a strategy used in modern diesel engines to reduce sooting [27]. The images show no significant differences in spray structure, but this may be due to the 3ms time lapse between injection pulses [Figure 13].

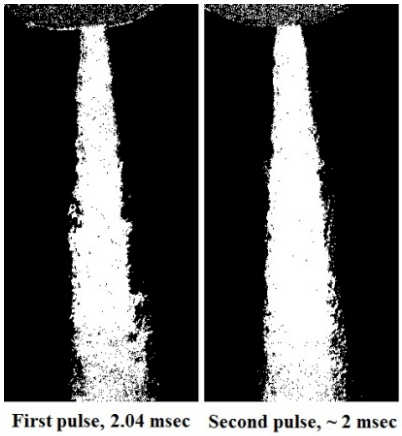

Figure 13: Images of a double-pulsed sequence of injections shows similar structure in each spray.

3.3 Effect of Charge Pressure on Dodecane Sprays

The next series of images were captured of dodecane injected into air at room temperature and increasing pressure [Figure 14]. Periphery shedding of the liquid core is seen at all pressures, but much less pronounced than what is seen at higher air temperatures [Figure 15]. These images revealed that the near-nozzle spray angle increased with increasing air pressure at cold temperatures. There was also an increase in the fluctuation of the spray angle with increased air pressure, as seen from the error bars in the inset graph.

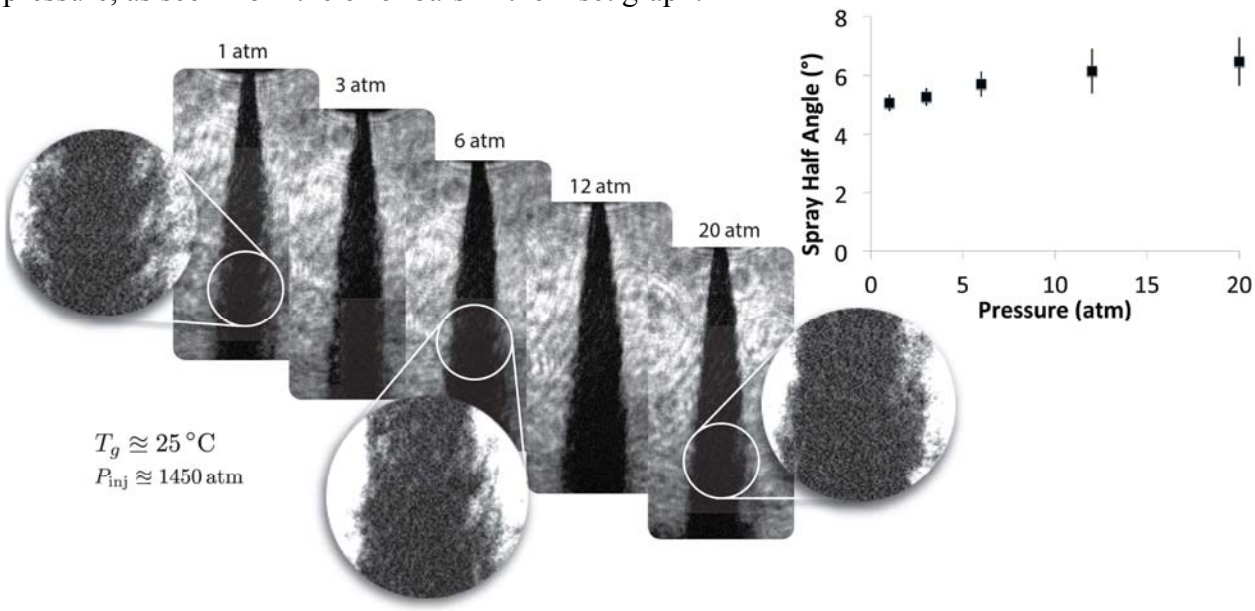

Figure 14: Images of dodecane at room temperature and increasing pressures. Balloons added to highlight shedding phenomena.

3.4 Effect of Charge Temperature and Pressure on Dodecane Sprays

The most relevant testing regime to diesel engine studies was the imaging of dodecane at high air temperatures and pressures. At these air temperatures, the liquid fuel is preheated in the injector to ~150°C. Dodecane was injected into air at 600ºC and pressures from 3-20 atmospheres. At the higher-pressure levels, conditions are representative of the environment found in actual diesel engines [Table 1]. The higher chamber pressure and temperature caused large density gradients in the pressure vessel making it impossible to acquire quality baseline images [Figure 9]. The images shown here have been converted to optical depth by taking the log of the image.

The captured images revealed many trends that varied with pressure and revealed breakup structures that to our knowledge have not previously been observed in the near-orifice region, but have been predicted by others [28]. Initial images revealed large differences in the observed structures compared to those observed at the same pressures but lower temperature [Figure 14]. Additionally, the observed spray cone angles increased with pressure [Figure 15], similar to the low temperature sprays [Figure 14]. Further examination revealed that the observed shedding structures developed nearer to the injector with increasing pressure [Figure 16]. In addition, it appears that the optical density of the spray seems lower during the period of time when the 'finger' structures occur, which may be indicative of evaporation and mixing within the spray cone.

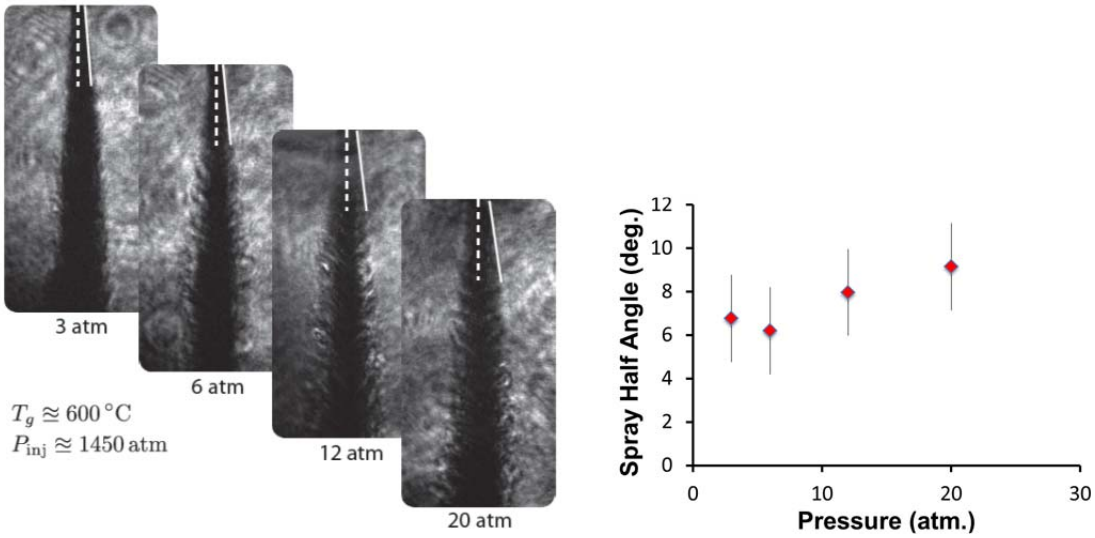

Figure 15: Example images which exhibit the trend of increasing cone angle with pressure (left) and averaged cone angle for all sprays (right).

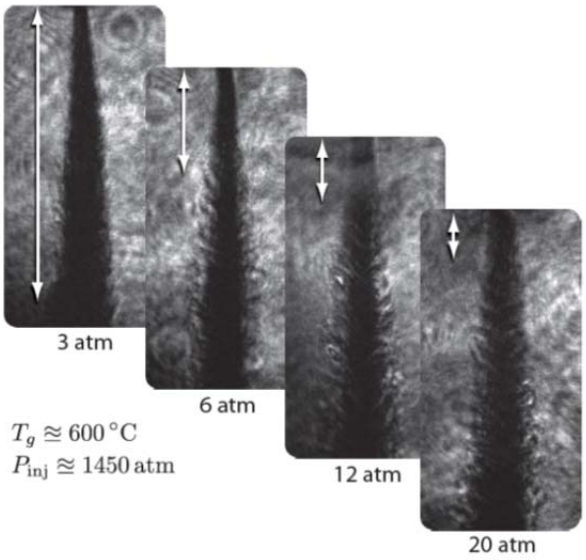

Figure 16: The visible start of the shedding structures varies with pressure.

A comparison of the spray cone angles of images taken at 20 atm and 25ºC and those taken at 20 atm and 600ºC reveal some interesting trends. Cone angle measurements were made of sprays over the entire injection event at the two aforementioned environmental conditions and plotted in Figure 17. The lower temperature spray reveals oscillation of the cone's angle, whereas the higher temperature spray initially oscillates but then settles to an almost constant angle. Interestingly, this temporal region corresponds directly with the existence of the 'fingerlike' structures caused by violent mass shedding. A similar trend is observed at 12 atm and 600ºC.

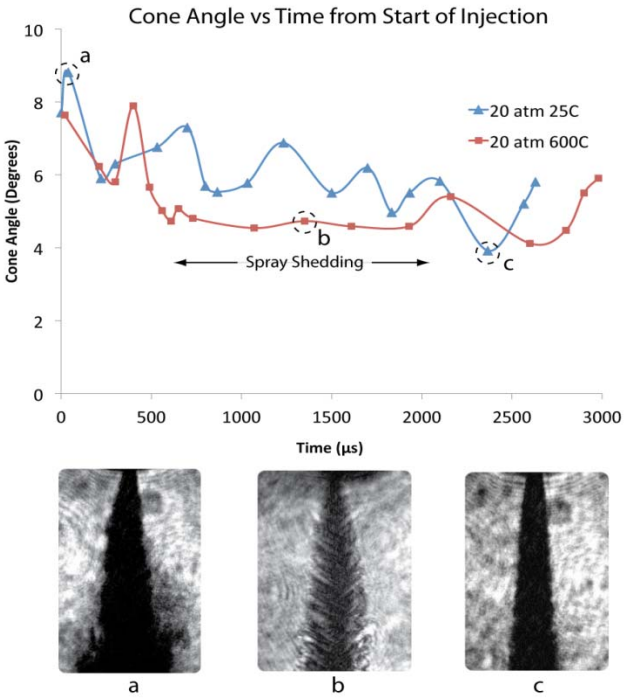

Figure 17: Measured spray cone angles as a function of time. Sprays were injected into a 20 atm environment at 25° and 600°C. The smooth region of the 600°C curve corresponds to the observation of spray shedding.

3.5 Spray Structure in a Biodiesel Surrogate

To investigate the effect of fuel type on the near-nozzle region of diesel sprays, methyl oleate was substituted for dodecane for a series of images. Methyl oleate ($C_{19}H_{36}O_2$) is a common surrogate for biodiesel. The resulting spray images were very clearly different than those of the low air temperature and pressure dodecane tests. Foremost, the spray cone was markedly wider in the methyl oleate images [Figure 18]. Additionally, the images reveal what appear to be large shedding structures along the periphery. This scale of shedding is not observed in the ambient dodecane images, but has been observed in high temperature and pressure dodecane sprays as discussed. The reason for these shedding structures in methyl oleate is not understood. In fact the increased viscosity of methyl oleate relative to dodecane should inhibit breakup [Table 2]. Further imaging of biodiesel surrogates is planned.

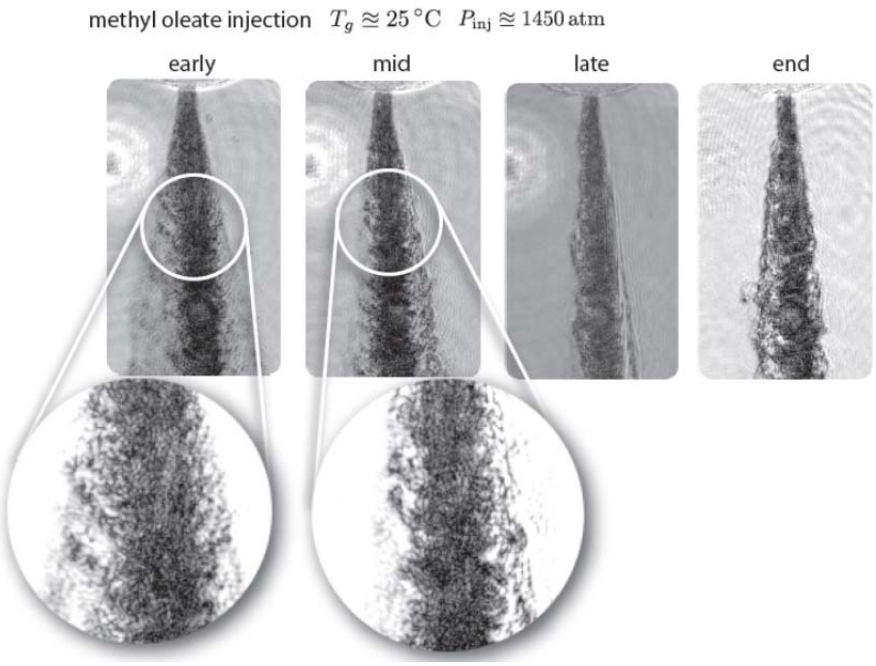

Figure 18: Images of methyl oleate which reveal a wider spray cone and peripheral shedding.

3.6 Ballistic Scattering

Ballistic imaging, as applied to date, is a line-of-sight technique that produces a shadowgram-like image of the line-integrated structures in the spray. Resolution normal to the line-of-sight is quite good; however, no resolution along the line-of-sight is achieved. In essence this means that the cross sectional area, presented as a map of the optical depth of the field, is imaged. The implication of this is that two objects that are separate in space but that present a joined cross sectional area along the line-of-sight will appear as a single object. Similar to the evolution from line-of-sight absorption measurements to spatially resolved fluorescence measurements; ballistic imaging is poised to progress from a line-of-sight format to a truly spatially resolved format.

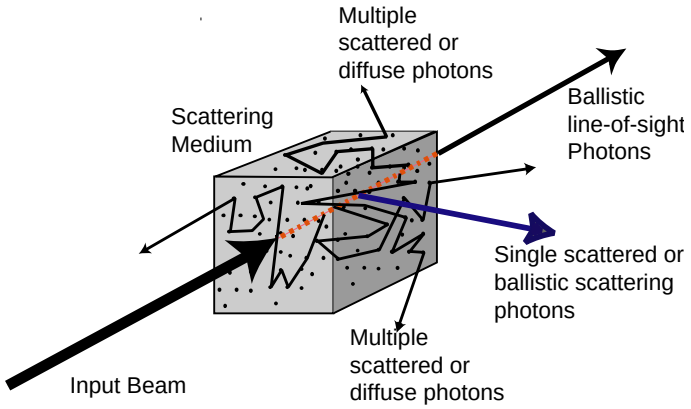

Figure 19: Schematic diagram of ballistic line-of-sight photons, ballistic scattered photons, and diffuse photons.

For highly scattering media, such as the near field of a diesel spray, the scattering signal from a laser sheet illuminated plane can be imaged onto a camera. As scattering in dense media suffers from the same problem as line-of-sight measurements, namely that multiply scattered or diffuse

photons obscure the image information associated with singly scattered or ballistic photons, ballistic photons must be separated from diffuse photons using a time gate. Figure 19 shows a generic ballistic line-of-sight and ballistic scattering photon path. Photons that pass through the media without scattering or any interaction are ballistic photons. Many photons are scattered several times; these are termed multiply scattered or diffuse photons, which can exit the material in any direction. Finally, singly scattered photons are labeled as "ballistic scattering photons." As with line-of-sight ballistic photons, ballistic scattering photons travel the shortest distance to the detector and can be separated from diffuse photons with an ultra-fast optical shutter. The scattering image of structures in the laser-illuminated field is carried by these ballistic or single scattered photons, which can be separated from the multiply scattered photons using an ultra-fast optical shutter.

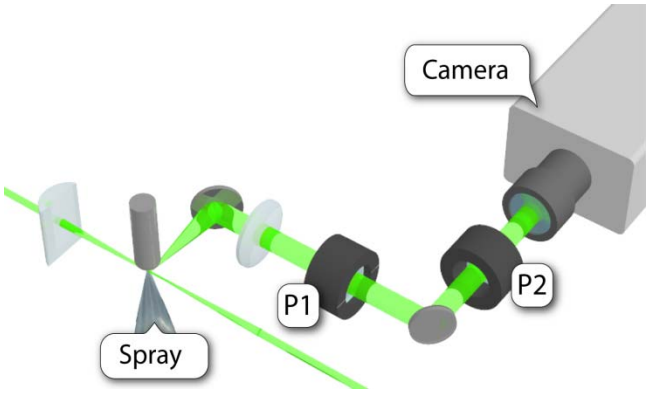

Figure 20: Optical setup for semi-ballistic scattering measurements. Laser sheet passes through spray and collected scattered light passes through polarizers P1 and P2.

To demonstrate the potential of this approach, a thin sheet (15 μm) of pulsed light was used to probe a dodecane spray. Light scattered perpendicular to the sheet was collected with imaging optics and passed through a polarizer (to block the majority of multiply scattered photons) before being captured with a camera (Figure 20). Note that this is not a scattering intensity based technique, rather, objects illuminated by the laser produce similarly shaped images at the imaging plane. For objects above the diffraction limit (typically stated as 3 μm for visible light), the size of the object will be directly represented in the camera image. This technique is referred to here as semi-ballistic; the next step is to add an OKE gate to produce a ballistic image.

Although further development is needed, early demonstrations of this concept have shown some promising results. Figure 21 shows two preliminary semi-ballistic scattering images taken of a dodecane spray in ambient air. The presence of voids and edge effects indicates the successful capture of ballistic photons, as these internal features of the spray would otherwise be averaged out through multiple scattering by surrounding droplets. Adding in the OKE shutter should provide additional spray structure details that are interior to the global structure observed.

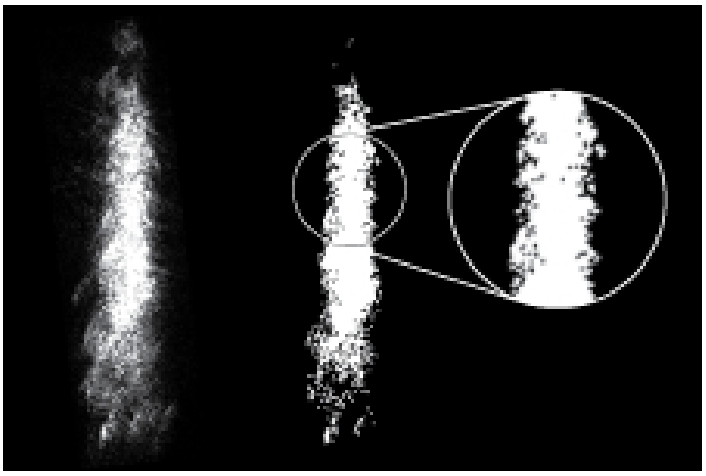

Figure 21: Scattering image taken at nozzle exit of a dodecane spray (1450 atm injection pressure) in an ambient air background. Image is approximately 4mm in height. Binary image (center, right) highlights spray edge structures.

The OKE gate timing for this application is potentially more sensitive since photons originating from the pulse entry side of the spray will arrive at the OKE gate (for an exact 90º imaging setup) before those from the pulse exit side of the spray by the propagation time for light through this distance (for a 3 mm wide spray, this time is approximately 10 ps). The first approach to this problem will be tuning the gate time to produce a high quality image of the two spray extremes and then determine if we can produce a gate that is of sufficient width to capture both spray edges *and* reject multiply scattered photons. Note that one of the advantages of this technique is the ability to control the OKE gate width over a range from ~7 ps to ~15 ps. If simple gate width control does not produce appropriate results, the production of imaging paths that naturally overcome the propagation delay of light through a spray will be explored (e.g. non-orthogonal light paths with appropriate depth of field or orthogonal light paths that include a wedge optic that produces a variable delay in the propagation).

The Continuum Leopard laser has sufficient energy in 1 ps of the total pulse width to produce approximately 8000 photons at the imaging plane from a 10 micron fluid element. Therefore, the energy to produce a scattering image is available and the gating techniques developed for line-of-sight ballistic imaging would be used. This improvement to ballistic imaging would enhance information acquired at the breakup region of the diesel spray since true spatial information in the jet breakup region would be acquired. The issue of sufficient beam intensity for the scattering is also addressed by the images shown in Figure 21; these images were taken with a non-optimized image system using 10% of the beam from the continuum Leopard (which therefore leaves 90% of the original beam for use as the OKE Gate beam).

4. Conclusions and Future Work

The first successful demonstration of picosecond ballistic imaging has been achieved. This technique has been applied to diesel injection sprays of dodecane, JP10 (not shown), and methyl oleate. Injection into ambient air reveals several trends in the near-nozzle region including oscillation in spray cone angle in time, fuel effects, and the impact of the injection pressure on spray cone angle. The first ballistic images of dodecane sprays into an environment typical of diesel engines demonstrate marked trends of cone angle fluctuation and significant mass

shedding. Structures imaged at high temperature and pressure bear resemblance to those predicted by the modeling community, and should help improve overall understanding of the underlying fluid dynamics. In addition, semi-ballistic scattering images reveal the potential to complement line-of-site ballistic images with orthogonal imaging of spray structures through scattering.

Future efforts will include both optical measurement development and data production for diesel systems. Optical diagnostic development will include extending the CSM ballistic imaging system from a line-of-sight measurement system to a spatially resolved imaging technique through ballistic scattering imaging. This extension will remove the ambiguities associated with a line-of-sight measurement and allow identification of structures that lie in the illuminated plane. Further planned extensions of the diagnostics include: 1) judicious use of probe wavelengths to facilitate probe features more typical of soot than of droplets (including multiple simultaneous probes to separate soot and droplet zones in the spray), and 2) incorporating short pulse time gating to established techniques such as fluorescence and exciplex fluorescence for application in the near-orifice region of the spray (these techniques have not been applied in the near-orifice due to multiple scattering effects).

Efforts in data production will include use the redesigned CSM Diesel Simulator to establish benchmark data sets with well defined boundary conditions and data over a wide operating parameter range for investigation of breakup mechanisms. Specifically, background gas density and temperature will be varied over a wide range to assess the importance of aerodynamic effects, and a range of spray nozzles will be used to assess the importance/role of cavitation in breakup. A comparative data set focused on spray breakup and ignition for diesel fuel (probably a range of certification fuels) and JP8 (again a range of fuels) will be produced. Examining the data from a perspective of the spray and the ignition at diesel relevant conditions is particularly interesting. In addition, ballistic images of the diesel fuel and JP8 in the near field would show the sensitivity of the near field to fuel properties.

Acknowledgements
The authors would like to thank ARO program manager Dr. Ralph Anthenien for his ongoing support of this work.

5. Bibliography

[1] T. E. Parker, L. R. Rainaldi, and W. T. Rawlins, "A comparative study of room-temperature and combusting fuel sprays near the injector tip using infrared laser diagnostics," *Atomization and Sprays*, vol. 8, no. 5, p. 565, 1998.

[2] W. D. Bachalo and M. J. Houser, "Phase/Doppler spray analyzer for simultaneous measurements of drop size and velocity distributions," *Optical Engineering*, vol. 23, no. 5, pp. 583–590, 1984.

[3] S. V. Sankar, B. J. Weber, D. Y. Kamemoto, and W. D. Bachalo, "Sizing fine particles with the phase Doppler interferometric technique," *Appl. Opt.*, vol. 30, no. 33, pp. 4914–4920, Nov. 1991.

[4] G. A. Ruff, L. P. Bernal, and G. M. Faeth, "Structure of the near-injector region of non-evaporating pressure-atomized sprays," in *27th AIAA Aerospace Sciences Meeting*, 1989, vol. 1.
[5] L. Arnone, F. Beretta, A. Tregrossi, A. D'Alessio, and F. Ossler, "Ensemble and time resolved light scattering measurements in isothermal and burning heavy oil sprays," *Symposium (International) on Combustion*, vol. 24, no. 1, pp. 1549–1555, 1992.
[6] F. Beretta, A. Cavaliere, and A. D'Alessio, "Ensemble laser light scattering diagnostics for the study of fuel sprays in isothermal and burning conditions," *Symposium (International) on Combustion*, vol. 20, no. 1, pp. 1249–1258, 1985.
[7] L. G. Dodge, D. J. Rhodes, and R. D. Reitz, "Drop-size measurement techniques for sprays: comparison of Malvern laser-diffraction and Aerometrics phase/Doppler," *Appl. Opt.*, vol. 26, no. 11, pp. 2144–2154, Jun. 1987.
[8] P. G. Felton, A. A. Hamidi, and A. K. Aigal, "Measurement of drop size distribution in dense sprays by laser diffraction," in *Proceedings of the Third International Conference on Liquid Atomisation and Spray Systems (ICLASS)*, London, England, 1985, vol. 2.
[9] Y. Yue, C. F. Powell, R. Poola, and J. Wang, "Quantitative measurements of diesel fuel spray characteristics in the near-nozzle region by using x-ray absorption.," *Atomization and Sprays*, vol. 11, no. 4, pp. 471–490, 2001.
[10] Z. Liu, K. S. Im, X. Xie, Y. Wang, X. Zhang, S. Moon, J. Gao, K. Fezzaa, M. C. Lai, K. Harkay, and others, "Ultra-Fast Phase-Contrast X-ray Imaging of Near-Nozzle Velocity Field of High-Speed Diesel Fuel Sprays," *ILASS-Americas, Cincinnati, Ohio, USA*, 2010.
[11] W.-K. Lee, K. Fezzaa, and J. Wang, "Metrology of steel micronozzles using x-ray propagation-based phase-enhanced microimaging," *Appl. Phys. Lett.*, vol. 87, no. 8, p. 084105, 2005.
[12] M. Linne, "Analysis of X-ray phase contrast imaging in atomizing sprays," *Experiments in Fluids*, vol. 52, no. 5, pp. 1201–1218, 2012.
[13] P. F. Flynn, R. P. Durrett, G. L. Hunter, O. C. Akinyemi, J. E. Dec, and C. K. Westbrook, "Diesel Combustion: An Integrated View Combining Laser Diagnostics, Chemical Kinetics, And Empirical Validation," 1999.
[14] M. Paciaroni, M. Linne, T. Hall, J. P. Delplanque, and T. Parker, "Single-shot two-dimensional ballistic imaging of the liquid core in an atomizing spray," *Atomization and sprays*, vol. 16, no. 1, pp. 51–70, 2006.
[15] M. Paciaroni and M. Linne, "Single-Shot, Two-Dimensional Ballistic Imaging through Scattering Media," *Appl. Opt.*, vol. 43, no. 26, pp. 5100–5109, 2004.
[16] M. Linne, M. Paciaroni, T. Hall, and T. Parker, "Ballistic imaging of the near field in a diesel spray," *Exp Fluids*, vol. 40, no. 6, pp. 836–846, Feb. 2006.
[17] S. Duran, J. M. Porter, and T. R. Parker, "Ballistic Imaging of Sprays at Diesel Relevant Conditions," in *Proceedings of the Twelvth International Conference on Liquid Atomisation and Spray Systems (ICLASS)*, Heidelberg, Germany, 2012.
[18] W. Hentschel, "Modern tools for diesel engine combustion investigation," *Symposium (International) on Combustion*, vol. 26, no. 2, pp. 2503–2515, 1996.
[19] M. K. Khair, "Progress in diesel engine emissions control," *Journal of engineering for gas turbines and power*, vol. 114, p. 568, 1992.
[20] J. B. Heywood, *Internal combustion engine fundamentals*. McGraw-Hill, 1988.
[21] D. Nehmer, "personal communication," Sturman Industries-2002.

[22] D. L. Siebers, “Scaling liquid-phase fuel penetration in diesel sprays based on mixing-limited vaporization,” *SAE technical paper*, pp. 01–0528, 1999.
[23] V. Diky, R. D. Chirico, C. D. Muzny, A. F. Kazakov, K. Kroenlein, J. W. Magee, I. Abdulagatov, J. W. Kang, and M. Frenkel, “ThermoData Engine (TDE) Software Implementation of the Dynamic Data Evaluation Concept. 7. Ternary Mixtures,” *J. Chem. Inf. Model.*, vol. 52, no. 1, pp. 260–276, Jan. 2012.
[24] J. J. Jasper, “The Surface Tension of Pure Liquid Compounds,” *Journal of Physical and Chemical Reference Data*, vol. 1, no. 4, pp. 841–1010, Oct. 1972.
[25] K. M. Doll, B. R. Moser, and S. Z. Erhan, “Surface Tension Studies of Alkyl Esters and Epoxidized Alkyl Esters Relevant to Oleochemically Based Fuel Additives†,” *Energy Fuels*, vol. 21, no. 5, pp. 3044–3048, Sep. 2007.
[26] W. A. Sirignano, *Fluid Dynamics and Transport of Droplets and Sprays*. Cambridge University Press, 1999.
[27] Z. Han, A. Uludogan, G. J. Hampson, and R. D. Reitz, “Mechanism of Soot and NOx Emission Reduction Using Multiple-injection in a Diesel Engine,” SAE International, Warrendale, PA, 960633, Feb. 1996.
[28] D. Jarrahbashi and W. A. Sirignano, “Acceleration Effects on Instability of High-Pressure Fuel Jets,” in *Proceedings of the Twelvth International Conference on Liquid Atomisation and Spray Systems (ICLASS)*, Heidelberg, Germany, 2012.